Available online at www.sciencedirect.com
SCIENCE DIRECT®
Infrared Physics & Technology 45 (2004) 349–364
INFRARED PHYSICS & TECHNOLOGY
www.elsevier.com/locate/infrared

Highly resolved transmission infrared microscopy in polymer science ☆

Gary Ellis *, Carlos Marco, Marian Gómez

Departamento de Física e Ingeniería, Instituto de Ciencia y Tecnología de Polímeros, Consejo Superior de Investigaciones Científicas, c/Juan de la Cierva 3, 28006 Madrid, Spain

Available online 18 March 2004

Abstract

Over the last few years, the use of synchrotron-based IR sources for high-resolution microspectroscopy has been a subject of great interest. The special characteristics of synchrotron radiation allow one to obtain high quality IR spectra at high spatial resolution using commercial grade IR microscopes situated at IR beamlines. The application of this technique to the study of polymeric materials is discussed, with examples from a series of heterogeneous polymeric materials, which include polymer blends and fibre-reinforced polymer composites, from studies undertaken at the MIRAGE Beamline, LURE, Paris, France.

Keywords: Synchrotron infrared microscopy; Polymer; Morphology; Composite

1. Introduction

Infrared spectroscopy is probably the most widely used structural tool for the characterization of polymeric materials. Polymers can be studied in a variety of forms, and are most commonly studied as thin films prepared either from solution or by pressing. Over the years, much attention has been paid to the development of sampling techniques which allowed the analyst to study increasingly more difficult samples, and one of the most demanding sampling problems has been the non-destructive study of small samples. Amongst the first solutions, the beam condenser accessory can be considered the most widespread, reducing a typical beam diameter of 8 or 10 mm in the sample area to a few mm. Combined with micro-sampling methods such as the KBr micro-press technique [1], and the diamond anvil cell [2] small polymer particles or fragments became accessible.

The first references in the literature on the combination of microscopy and IR spectroscopy appeared before the Second World War, but it was not until the early 1950s [3,4] that the first successful applications of the technique for the characterization of microscopic samples emerged. Infrared microscopy, or infrared microspectroscopy as it is often called only became fully commercially

☆ Presented in part as an Invited Lecture at the International Workshop on Infrared Microscopy and Spectroscopy with Accelerator Based Sources, July 8–11, 2003, Lake Tahoe, CA, USA.

* Corresponding author. Tel.: +34-915622900; fax: +34-915644853.
E-mail address: gary@ictp.csic.es (G. Ellis).

1350-4495/$ - see front matter
doi:10.1016/j.infrared.2004.01.015

available in the early 1980s, due to significant technological advances in Fourier transform infrared spectroscopy, and related data processing hardware and software. Since then it has made significant impact in a wide range of areas in polymer science, and examples include identification and characterization of polymers and polymer contaminants, forensics, orientation studies, etc., and a number of reviews and monographs which refer to polymer applications are available in the literature [5–11].

Modern systems employ reflective Cassegrain or Schwarzchild objectives and condensers which focus the IR radiation on the sample and collect the transmitted or reflected light for delivery to the detector, generally a cryogenically cooled mercury cadmium telluride (MCT) device. Variable apertures are situated at one or more conjugate image planes to allow specific selection of the area to be studied. The development of sophisticated software and hardware in these systems, such as the use of computer controlled *xy* translation stages, allow not only the characterization of specific points on a sample, but also enable the analyst to generate infrared spectral maps of whole areas of a sample, providing spatial or topological chemical and structural information over selected regions of a given specimen. With specialized optics such as attenuated total reflectance (ATR) objectives, grazing angle objectives, etc., the study of polymeric systems at the microscopic level is now almost routine.

The spatial resolution of the microscope can be controlled by changing the size of the apertures. However, the highest spatial resolution of an infrared microscope is not defined by the size of the field apertures, but rather by the diffraction limit of the radiation. The resolution limit, Δl, or the minimum resolvable separation of two points on the sample, is usually described by the Rayleigh criterion, which is given by Abbe [12] as

$$\Delta l = \frac{0.61\lambda}{\mathrm{NA}} \tag{1}$$

where λ is the wavelength of the infrared radiation, and NA is the numerical aperture of the microscope system. Over the mid-infrared region, between 4000 and 400 cm^{-1}, the wavelength varies between 2.5 and 25 μm. So if we consider a microscope with an ideal numerical aperture of 1, we would find at 1000 cm^{-1}, a maximum spatial resolution of around 6 μm. However, if we close the field apertures down to 6 μm in a typical IR microscope, the result we obtain is poor. This is because the amount of infrared radiation passing through such a small aperture is too low, and the signal-to-noise ratio falls dramatically. Due to the aforementioned noise limitations, the best spatial resolution available in an IR microscope is generally quoted as around 10 μm, and should be considered more as a practical limit, independent of wavelength considerations.

Various alternative sources which provide higher energy through small apertures have been considered. An tuneable infrared diode laser has been used in an microscope to study contaminant diffusion in a multi-layer polymer [13], and diffraction-limited resolution was claimed for IR images obtained from bands which fall within the tuneable bandwidth, between 6.2 and 6.5 μm.

Spatially resolved vibrational spectra can also obtained using Raman microscopy, which is now an extensively used technique, and with modern confocal microscope systems and visible laser sources a lateral spatial resolution of around 1 μm can be routinely achieved [14]. However, in many materials, and especially multiphase polymer systems, its use can be limited due to problems of absorption and fluorescence.

Other complimentary microscopy techniques, such as electron energy loss spectroscopy (EELS) in an electron microscope [15], near-edge X-ray absorption fine structure (NEXAFS) in an X-ray microscope [16], or scanning force microscopy (SFM) [17], can also provide either direct or indirect mapping or imaging of polymeric materials at even higher spatial resolution.

EELS probes the local chemical and electronic structure of carbon-based materials providing information from the inner and outer shell electrons. With sufficient elemental discrimination, images can be generated routinely at spatial resolutions of around 100 nm, and sub-nanometre resolution has been reported [18]. However, the major disadvantage in the study of polymers is the significant electron beam damage, although

various examples of the information available from polymers can be found in the literature [19–21].

Soft X-ray spectromicroscopy using synchrotron radiation has found extensive applications in the polymer field since NEXAFS was first used to examine polymer blends in 1992 [22], and a wide range of multiphase polymers have already been studied [23,24]. Both quantitative chemical information, and morphological or structural information, such as orientation [25–27], is available, and spatial resolution better than 40 nm can now be achieved [28], with significantly lower level of beam damage than that observed in EELS.

The advances in SFM now allow one to measure surface topography in polymer systems in at a spatial resolution in the 5–20 nm range, and a number of sophisticated techniques are available to obtain specific chemical and structural information [17].

Using near-field techniques, a number of high spatial resolution spectroscopic and imaging methods have been recently developed. For example, with near-field optical microscopy in the infrared region between 1 and 10 μm, combined with a free-electron laser, a spatial contrast of between $\lambda/6$ and $\lambda/40$ has been observed [29]. Near-field Raman imaging has also been developed combining Raman microscopy and AFM, and 50 nm spatial resolution can be achieved with enhanced tips [30,31]. Infrared imaging with 100 nm spatial resolution has been reported from polymer blends combining near-field microscopy with AFM, using aperture-less scattering tips irradiated with an IR laser [32,33]. With this type of arrangement, a spatial resolution of 17 nm ($\lambda/600$) was previously reported from a Au–Si grating [34]. Using a broadband laser source and a focal-plane array spectrometer, near-field mid-infrared absorption spectra have also been performed on a polymer nanocomposite [35].

Finally, using a novel probe infrared spectra of polymer films have been obtained in an AFM at a spatial resolution of around 100 nm, by detecting photothermally induced temperature fluctuations at the sample surface using a miniature wire resistance thermometer [36,37].

However, the ability to obtain higher spatial resolution in conventional IR microscopy is clearly of great interest, because of the grand versatility of the technique, which can provide highly detailed chemical and structural information through non-destructive analysis, either by simple transmission measurements, or by the use of relatively cheap specialized reflection sampling methods.

The use of synchrotron based sources for IR spectroscopy was first reported by Williams over 20 years ago [38]. Synchrotron radiation obtained from a bending magnet in a storage ring provides a highly coherent broadband IR source which covers the whole IR region. Its extraordinarily high brightness can provide more than three orders of magnitude improvement in intensity [39,40], and its almost linear broadband spectral coverage over the whole IR region, which makes it an ideal IR source [41]. The importance of this discovery was soon recognized, and the improved beam stability of modern synchrotron sources along with a manageable beam size allowed it to be efficiently coupled to an IR microscope. The first IR microscopy beamline was built at Brookhaven National Laboratory, New York in 1993 [41–43]. At present there are more than a dozen IR microscopy beamlines, active or under development, throughout the world.

The access to higher spatial resolution infrared microscopy has opened up a whole new line of studies over a wide area of disciplines [44–75]. Examples include biological or biomedical systems [44–53], food science [54–57], geology and geochemistry [58–61], electrochemistry and surface science [62–65], high pressure studies [66,67], industrial research and forensics [68–73], and time-resolved spectroscopy [59,74]. However, to date only a few examples for the study of synthetic polymers have appeared in the literature [75–79].

This article considers some aspects of the study of polymer blends and composites using synchrotron infrared microscopy, where the improved spatial resolution is a considerable advantage. Particular emphasis has been placed on materials based on a polypropylene matrix, and the synchrotron IR data obtained is compared with those obtained from a conventional IR microscope, a confocal Raman microscope, and a modern infrared imaging system.

2. Experimental

2.1. Materials

The thermoplastic matrix used was a commercial isotactic polypropylene (REPSOL-YPF, Madrid, Spain) with a molecular weight $M_v = 164,000$ and 95% isotacticity determined by solution NMR spectroscopy [80]. Different thermal histories were applied to the samples, as described in the text.

Two blends of polypropylene and nylon-6 were studied with a composition of 70% polypropylene and 30% nylon-6. In one of the blends 10% by weight of the polypropylene component was replaced by an interfacial agent, Exxelor (Shell), a graft copolymer of polypropylene and maleic anhydride. The blends were prepared by extrusion, and are described elsewhere, along with the rheological and morphological properties [81]. Microtomed samples, of approximately 20 μm thickness, were taken from the extruded blends and mounted on a home-made microscope sample holder.

Model fibre-reinforced composites were prepared by sandwiching single-filament (23–26 μm diameter) Vectra A950 167 TEX liquid crystal polymer fibres (Hoechst), between two thin iPP. Vectra A950 is a thermotropic copolyester of 73% hydroxybenzoic acid and 27% hydroxynaphthoic acid. Full details of the sample preparation technique are given elsewhere [79]. The model composites were given specific thermal histories in a Mettler FP82HT (Mettler-Toledo) microscope hot stage, after erasing any prior thermal history in the matrix [80]. Some of the LCP fibres were pulled slowly at fixed temperatures and a constant rate during crystallization, and observed using a Zetopan Pol polarising microscope (Reichert). After crystallization and cooling to room temperature, the specimens were then carefully removed from the glass microscope slides and mounted on cards with adhesive tape.

2.2. IR and Raman microscopy

The infrared spectra reported were recorded in all cases in the transmission mode from free-standing thin polymer films. A spectral resolution of 4 cm^{-1} was used in all cases. Three different microscope systems were employed:

System 1. Conventional IR spectroscopy and IR microscopy was undertaken on a Spectrum GX 2000 FTIR spectrometer, with an i-Series IMAGE microscope (Perkin Elmer), and analysed using Spectrum Software (Perkin Elmer). The microscope incorporates three permanently aligned Cassegrain objectives, with a numerical aperture (NA) of 0.6.

System 2. Microscopic infrared imaging was performed on a Spotlight 300 IR Imaging System (Perkin Elmer) coupled to a Spectrum One FTIR spectrometer (Perkin Elmer), and analysed using Spectrum Spotlight and Hyperview software (Perkin Elmer). The Spotlight is based on fixed 0.6 NA Cassegrains, but incorporates a novel optical system which includes a dual detector which combines both imaging and single point spectra modes [82].

System 3. Synchrotron IR microscopy was undertaken at the MIRAGE Beamline (SA5) of the SuperACO ring at LURE, Orsay, Paris. The Beamline incorporates a Nic-Plan IR microscope coupled to a Magna 560 FTIR spectrometer (Thermo-Nicolet). The Nic-Plan microscope uses two Schwarzchild objectives, the upper objective with a numerical aperture, NA, of 0.58 (15× magnification) and the lower objective with a NA of 0.71 (10× magnification). It employs confocally arranged knife-edge field-stop apertures which can be adjusted to around 3×3 μm. The majority of the measurements were performed using a single aperture (upper). Sample positioning and mapping operations are made with a digitally controlled *xy* motorised sample stage, and data is recorded and analysed using the Atlμs and Omnic E.S.P. software (Thermo-Nicolet). More details of the instrument and the coupling of the SR beam from the storage ring can be found elsewhere [83].

System 4. Raman spectra were obtained on a Renishaw RM100 confocal Raman Microscope (Renishaw), with argon ion laser excitation at $\lambda_0 = 514.5$ nm and a laser power at the sample of 4 mW focused on the sample by a 50× N-plan objective lens (Leica). Raman spectra were recorded with a resolution of 4 cm^{-1} from films

placed on a glass microscope slide without a cover slip, with an acquisition time of 20 s at each sample position.

3. Results and discussion

The vast majority of polymeric materials are, by nature, heterogeneous. If we consider a semicrystalline polymer, it contains both crystalline and amorphous material, and can develop complex superstructures in which the different domains are arranged. Depending on the thermomechanical history imposed on the material, it can also show anisotropic properties, and in some cases polymorphism. In addition, most application-grade polymers are not simply homopolymers, but are multi-component systems. These include polymer blends and composites, and also a wide range of additives that improve or enhance the materials properties, such as organic or inorganic fillers, nucleating agents, interfacial agents, antioxidants, etc., not forgetting the possible presence of contaminants such as catalyst or monomer residues, foreign particles and process degradation products.

In the characterization of these complex systems, the determination of parameters such as the composition or the orientation by bulk measurements often does not give sufficiently precise information on the nature of the system. For example, if we consider the optical properties of a semicrystalline polymer film, it is clear that the measurement of the size and distribution of the crystalline domains is fundamental to the understanding of both the transparency of the film, and its mechanical properties [84]. For this reason there is an important need to be able to obtain spectroscopic information from polymeric material at high spatial resolution.

Infrared microscopic mapping is well documented, and can provide spatially resolved information when used over representative areas of a sample. IR spectral maps can be obtained by either point-by-point raster scanning over a defined sample area, or more recently by spectral imaging [77,85]. The timescale of the measurement in static point mapping is defined by the step size of the microscope stage between each measurement point, which is often the smaller or equal to the aperture size. Thus, a compromise must be reached between the aperture size, spectral accumulation time, and size of the representative area on the sample in order to make microscopic mapping practical [86].

Until recently, the best spatial resolution available for the study of polymeric materials by infrared microscopy has been limited to aperture sizes of 10–15 μm. Indeed in many systems even larger apertures are preferred in order to be able to perform spectral mapping with good signal-to-noise ratios over reasonable timescales. However, the use of high brightness synchrotron IR radiation in a microscope has greatly improved the quality of spectra obtained through apertures below 10 μm. Carr [74,87] showed that the spatial resolution synchrotron infrared microscopy was indeed diffraction limited rather than aperture limited, and pointed that the best spatial resolution for a given wavelength is obtained in the confocal arrangement. Dumas et al. [75] demonstrated that using a synchrotron source, spectra could even be recorded through apertures considerably smaller than the diffraction limit of the radiation.

We have studied a series of polymeric materials, including homopolymers, polymer blends and composites in order to evaluate the possibilities for application in the field of polymer science.

Fig. 1a shows the spectrum recorded from an application grade polymer blend based on isotactic polypropylene using conventional IR microscopy, with a 100 μm × 100 μm aperture, using system 1. This polymer is a multi-component system which includes a propylene–ethylene copolymer matrix, a polyethylene homopolymer, a filler (talc), and a series of additives, and a number of components can be clearly identified. Fig. 1b shows a spectrum of the same sample obtained at the MIRAGE Beamline (system 2) through a 3 μm × 3 μm aperture. Clearly, the signal-to-noise ratio is lower, and particularly at lower wavenumber the effect of the small aperture can be seen. The characteristic doublet at around 720 and 730 cm^{-1}, which corresponds to the CH_2 rocking modes of crystalline polyethylene [88] appears to be reduced to a single

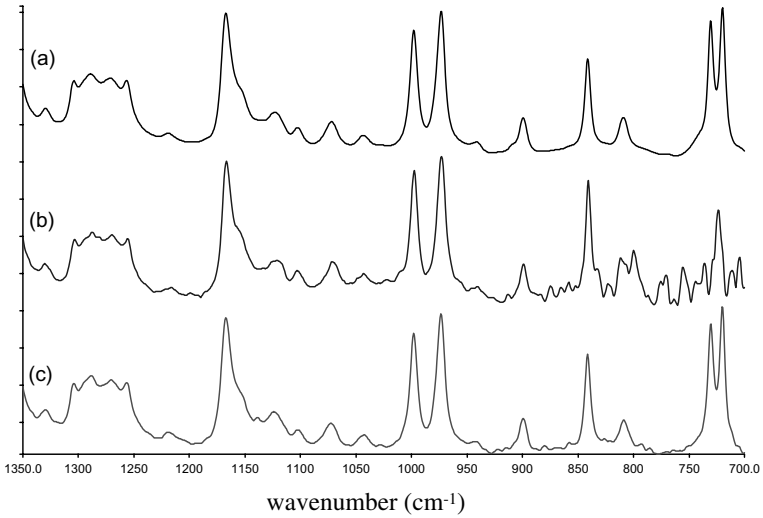

Fig. 1. Micro-IR spectra of a commercial high-impact iPP blend with different aperture sizes; (a) 100 μm (globar), (b) 3 μm (synchrotron), and (c) 15 μm (globar).

peak, and is of lower relative intensity than in the spectrum in Fig. 1a. If the spatial resolution was aperture limited, the difference in relative intensity could be due to variations in the polyethylene domain size and distribution in the sample, i.e. sample heterogeneity. However, in order to understand these differences it is fundamental to consider the diffraction limit for the bands of interest.

Table 1 shows the calculated diffraction limits over a range of wavenumbers for the Nic-Plan microscope using both single and dual aperturing. It is important to point out that even for an ideal optical system without aberration, the diffraction limit at 720 cm^{-1} a single aperture would correspond to 14.6 μm, almost 5× the aperture size employed. If we consider the spectrum in Fig. 1c, recorded on system 1 employing a 15 μm × 15 μm aperture, we observe that it is identical to that obtained in Fig. 1a. Thus we must conclude that using very small apertures not only increases the noise level, but can also distort the relative intensities observed in the spectra. In this case, over almost the entire spectrum the aperture size is smaller than the calculated diffraction limit, however, the distortion in intensity is only noticeable below around 800 cm^{-1}.

On a practical level, by using apertures below the diffraction limit of the band of interest, one is throwing away energy unnecessarily [74,87]. In principle, in order to obtain the best quality results, one should attempt to match the aperture size to the diffraction limit at the wavenumber of interest. For example, if we were interested in mapping a cyano group at 2235 cm^{-1} a single aperture with a size of around 5 μm × 5 μm would be suffice, whereas for a carbonyl group, the best aperture would be 6 μm × 6 μm. For polymer spectra of the fingerprint region, we have found an aperture size of 6 μm × 6 μm to be a good compromise between the best spatial resolution and the optimum energy throughput and signal-to-noise ratio.

Although there are some suggestions that when enough energy is available over-aperturing may be advisable to minimise diffraction effects at the aperture, it has demonstrated that there is no resolution advantage to be gained [11,87]. Further, since distortions can be introduced in the lower frequency region, as we have pointed out previously, over-aperturing is not recommendable. However, since it is often the case that information is required simultaneously from several bands over the whole spectrum, it is clear that it is important to control the aperture size ratio to avoid spectral distortions, and further study is required to quantify these effects when using small apertures.

Table 1
Diffraction limits calculated for the Nic-Plan microscope at the MIRAGE beamline for single and dual aperturing

Wavenumber (cm^{-1})	Wavelength (μm)	Abbe limit	
		Single aperturing	Dual aperturing
4000	2.5	2.2	1.9
3300	3.0	2.6	2.3
2938	3.4	2.9	2.6
2235	4.5	3.9	3.5
1750	5.7	4.9	4.4
1650	6.1	5.2	4.7
1600	6.3	5.4	4.8
1375	7.3	6.3	5.6
1000	10.0	8.6	7.8
800	12.5	10.8	9.7
730	13.7	11.8	10.6
720	13.9	12.0	10.8
650	15.4	13.3	11.9

On the contrary, it is generally accepted that over-sampling, i.e. using map step sizes smaller than aperture size, has been shown to be advantageous for obtaining sharper mapping data from details close to the diffraction limit [11].

3.1. Polymer blends

If we consider a polymer blend system based on isotactic polypropylene (iPP) and the polyamide, nylon-6, we can observe by scanning electron microscopy (SEM) that in a simple binary blend the minor component, nylon-6, forms spherical domains within the iPP matrix, Fig. 2a. This occurs because these polymers are incompatible systems, and the interfacial energy barrier is very high. This type of blend is known as an immiscible system, as is indeed the case for the majority of the commercial polymer systems. We have recorded spectra using a conventional microscope, system 1 (see Section 2), through a 20 μm square aperture over a 400 μm × 300 μm region of microtomed samples of this blend. If we compare the relative intensity (integrated area) of the amide I mode carbonyl stretching vibration at 1640 cm^{-1}, with that of the CH_2 deformation modes at around 1375 cm^{-1}, in the axonometric plot in Fig. 2a, the highest points, or peaks, correspond to the nylon-6 rich zones, whereas the lowest, or troughs, correspond to the iPP matrix. In order to improve the physical properties of this type of blend, interfacial agents are often employed. Fig. 2b shows a SEM microphotograph of the same blend composition compatibilized with a PP-maleic anhydride graft copolymer. The use of this agent has been shown to increase the dispersion of the nylon-6 and improve adhesion between the phases, leading to a more homogeneous system with improved physical and mechanical properties [81]. In the corresponding axonometric plot for the compatibilized blend, with the same *z*-axis scale as for Fig. 2a, it can be clearly observed that the difference in relative intensities is much smaller over the whole area, corresponding to a more homogeneous system. The higher average relative intensity is probably due to the formation of new amide type bonds during the compatibilization process [81], and their little variation indicates that the size of the domains has been significantly reduced, to below the resolution defined by the 20 μm apertures.

We have examined an area of 30 μm × 30 μm on the same samples using synchrotron IR microscopy (system 3), and Fig. 3a and b represent the axonometric plots for both the non-compatibilized (N) and compatibilized blends (C), respectively. In the upper part of each figure, the same band intensity ratio was employed as the plots in Fig. 2, using a single field stop aperture of 3 μm × 3 μm, with 3 μm steps of the *xy* translation stage. A relatively clear region between various polyamide domains in the N-blend, and a clean representative area for the

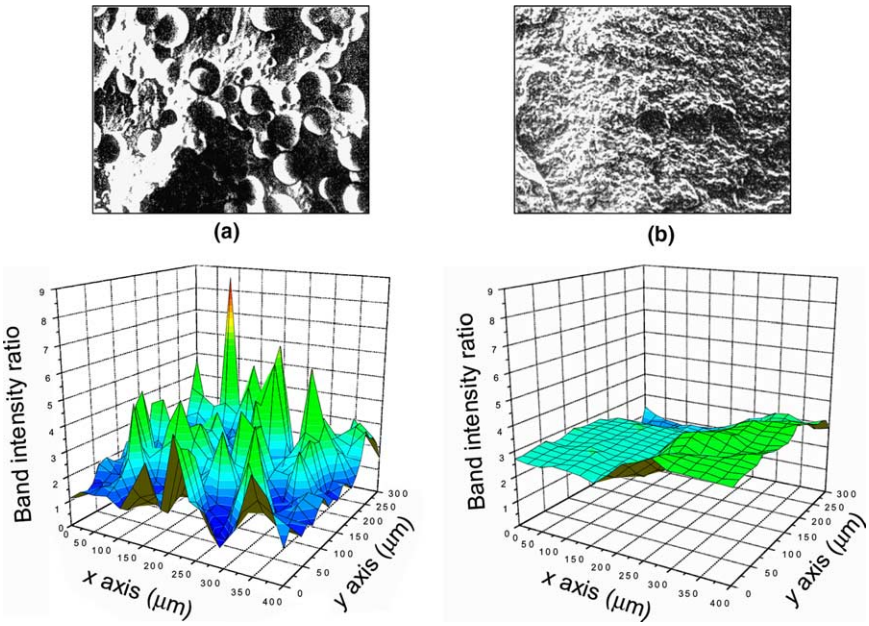

Fig. 2. SEM and IR band ratio maps (1640 cm^{-1}/1375 cm^{-1}) for iPP/nylon-6 70/30 blends: (a) simple binary blend and (b) binary blend compatibilized with PP-*g*-MAH interfacial agent.

C-blend were mapped. In the lower part of the figures, the broad amide N–H stretching vibration at around 3300 cm^{-1} was ratioed to the band at stretching vibration a 2938 cm^{-1}. Additionally, in the graphs for the C-blend, a contour map is also shown at the base of the *z*-axis.

As was previously observed, there are large differences in the relative intensities between the N-blend and the C-blend for both band ratios, showing the latter to be a much more homogeneous sample. However, there appears to be more detail in the plots, and in particular the contour maps obtained from the higher frequency band ratio. Taking into account that both band ratios are measuring the same phenomenon—the distribution of amide bonds in the system—we must attribute these differences as being due to the diffraction limits defined by the vibrational frequencies. The spatial resolution limit for the 1640 cm^{-1}/1375 cm^{-1} band pair is defined by the Abbe limit for the band of lowest frequency, and corresponds to 7.6 μm, whereas for the 3300 cm^{-1}/2938 cm^{-1} band pair it corresponds to less than half, at 3.6 μm. The increase in detail in both of the lower plots is due to the fact that the aperture size is more closely matched to the diffraction limit. However, in order to be able to consider differences in concentration or domain distribution from a more quantitative perspective, we must also consider the possible differences which can arise in the absorbance values for the bands as a function of the band frequency. As well as the possibility of distortions in the relative intensities with aperture sizes well below the diffraction limit, we must also consider that the sampled path length varies with frequency, and is also a function of diffraction, and the absorbance of IR bands has recently been shown to be sensitive to the aperture size in IR microscopy [89]. This is a subject of great importance, and will be discussed at a future date.

3.2. Crystalline morphology

The crystallization of polymers can give rise to a number of different crystalline superstructures, the most common being the spherulite. This is so-called because under natural crystallization conditions, for example dynamic crystallization from the molten state, the polymer chains organise themselves in crystallites which branch out radially

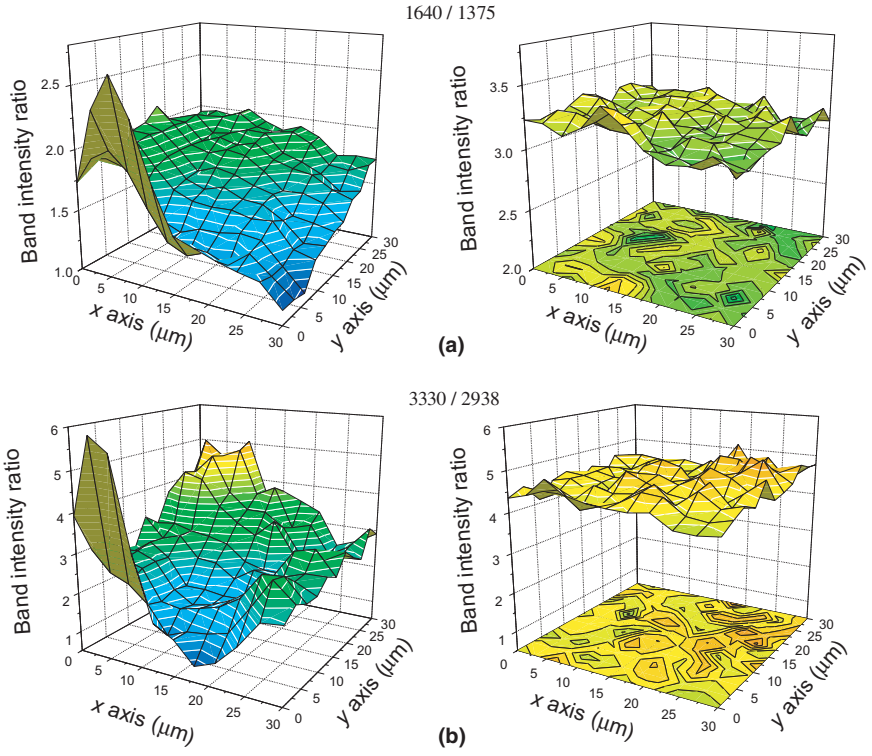

Fig. 3. Axonometric plots of IR band ratios of an area 30 μm × 30 μm of (a) N-blend and (b) C-blend. Upper plots use 1640 cm^{-1}/1375 cm^{-1} band ratio, lower plots use 3300 cm^{-1}/2938 cm^{-1} band ratio.

from the nucleation site in three dimensions. Various structural levels exist. The thickness of polymer crystallites can vary between 5 and 200 nm, whereas the size of a spherulite can vary between 0.5 and 500 μm, depending on the type of polymer and its crystallization conditions. Synchrotron IR microscopy is ideally suited to examine the nature of spherulite structure.

3.2.1. Polymorphism

Isotactic polypropylene can form various crystalline modifications depending on its thermal and processing history. The monoclinic or α-form is the most common, and is that which occurs under normal processing conditions. The second most common is the trigonal or β-form, which can be generated by temperature gradients or shear conditions, or can be activated by nucleating agents or surfaces [90]. Recently we have shown that subtle differences in the IR spectra of the α- and β-forms of iPP can allow us to differentiate between crystalline polymorphs [86,91], including the microscopic discrimination between individual spherulites.

Fig. 4 shows a polarised optical microphotograph of an area of a sample of polymorphic iPP, where the highly positively birefringent structure in the centre of the field corresponds to a β-spherulite. The darker negatively birefringent α-spherulites surround it. Using the 1330 cm^{-1}/1168 cm^{-1} band relationship, previously described as sensitive to α-/β-polymorphs [91], we can construct a high resolution IR false-colour contour map of the area marked A on the microphotograph, Fig. 5a, and can easily differentiate between the two crystal forms. Clearly, depending on the band relationships we employ, we can obtain information on other important parameters, such as the crystallinity and orientation of the sample [78]. This map was obtained with a globar source through a 10

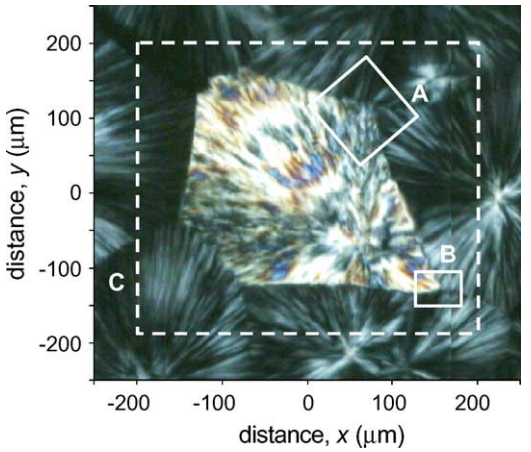

Fig. 4. Polarised optical microphotograph of polymorphic iPP. The boxes marked A, B and C correspond to mapped zones described in Figs. 5 and 6.

μm × 10 μm single aperture on system 1, and using a 2 min accumulation time at each data point took around 3 h obtain.

We have used similar subtle differences in the CH_2 and CH_3 stretching modes in the Raman spectra recorded on a Raman microscope (system 4), from area B of the sample, Fig. 5b. Curve fitting routines were used to isolate the Raman band at 2920 cm^{-1}, an asymmetric stretching vibration of the methylene group which is sensitive to the presence of the β-phase of iPP, and both the peak intensity and full width half maximum (FWHM) were analysed over an area of 50 μm × 34 μm, mapped at a lateral spatial resolution of 1 μm. Both methods provide a clear differentiation between the β-iPP spherulite and the surrounding α-iPP spherulites. Although quality of the differentiation in the data obtained is spectacular, the only disadvantage was the timescale of the measurement. Since the band of interest was one of a large group of overlapping frequencies, and the spectroscopic differences between the two crystal forms are subtle, a high signal-to-noise ratio was required for each data point in order to obtain reliable band deconvolution. Thus, several hours were employed in order to cover such a large sample area at high spatial resolution. It is important to point out that in other systems where bands of interest are well-defined and do not

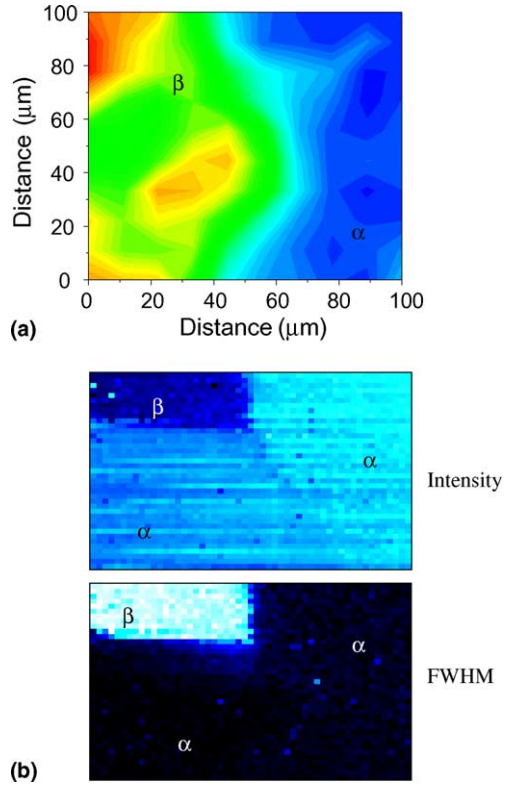

Fig. 5. (a) IR false colour contour image of area A, dimensions 100 μm × 100 μm. Map constructed using the 1330 cm^{-1}/1168 cm^{-1} band ratio with 10 μm × 10 μm aperture, and (b) confocal Raman point mapping images of the intensity and FWHM of the 2920 cm^{-1} band over area B, dimensions 50 μm × 34 μm.

overlap, sampling times can be significantly reduced, and Raman global imaging methods can be employed to obtain lower resolution images in a matter of minutes.

The same sample was also analysed using an IR Imaging System (system 2). Fig. 6a shows the false-colour contour map obtained from the area C marked on Fig. 4 using the 1330 cm^{-1}/1168 cm^{-1} band ratio. In this case we can obtain an IR image of the whole of the β-iPP spherulite. The extra magnification of the image in this microscope provides a pixel resolution of 6.25 μm, and the high sensitivity of the smaller detector element provides data of very good quality. When we examine examples of the individual spectra from the single pixels indicated by the arrows, Fig. 6b, the quality of the data obtained from the imaging

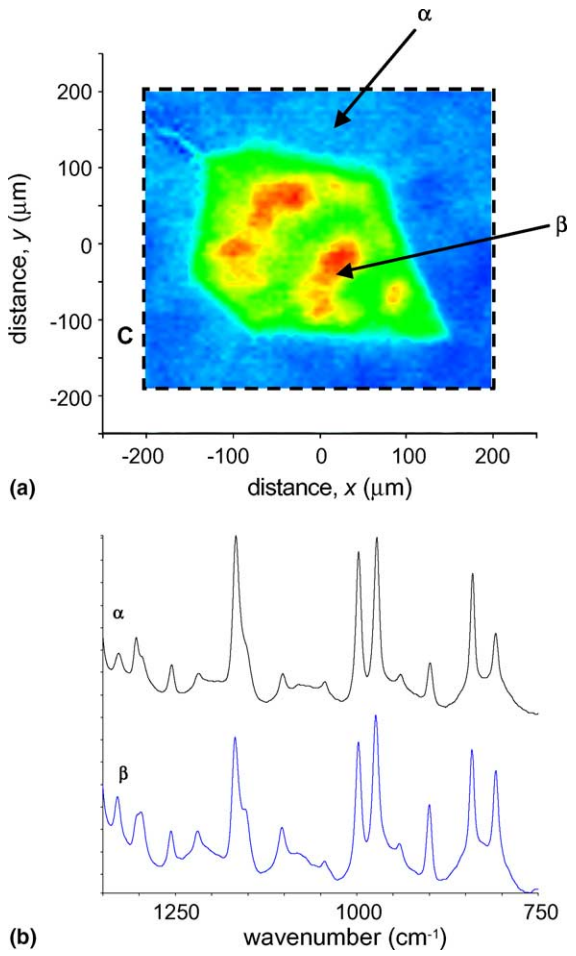

Fig. 6. IR imaging of polymorphic iPP (a) 400 μm × 388 μm map constructed using the 1330 cm^{-1}/1168 cm^{-1} band ratio, with 6.25 μm pixel resolution in the image, and (b) individual spectra corresponding to α-iPP and β-iPP taken from the positions marked.

microscope is comparable to that obtained from the synchrotron IR system over the fingerprint region of the spectrum. Thus, detailed maps can be obtained over large representative areas of the sample in a relatively short measurement times which in this case, for an area of 400 μm × 388 μm, was around 25 min.

Using synchrotron IR microscopy, we can demonstrate that is possible to obtain more detailed information from within the spherulites. It is important to point out that the synchrotron beam is highly polarised, and the relative band intensities in the spectra of anisotropic polymeric systems will depend on the orientation of the sample with respect to the electric vector of the beam. This sensitivity has already been demonstrated within both α- and β-spherulites for one of the band relationships shown to be characteristic of the polymorphic content [91]. If we record a series of spectra at fixed distance, r from the centre, or nucleus, of a given spherulite and at variable angle, θ, Fig. 7a, we observe that the relative intensities of a number of bands in the spectra vary as a function of the angle. This is because the spectra contain information on the relative orientation of the polymer chains within the crystalline superstructure. If, for example, we consider the absolute intensity of crystalline vibrational modes of iPP whose dipole moments lie at a known angle with respect to the polymer chain axis, and plot these versus angle, we obtain the graph observed in Fig. 7b, where a periodic variation in intensity as a function of the angular position within the spherulite is observed. The 840 cm^{-1} band is associated with methyl group rocking and skeletal stretching vibrations [92], with a dipole moment considered to be almost parallel to the polymer chain axis [93].

It is important to note from the observations of the variations in intensity of the 840 cm^{-1} band that the average orientation of the polymer chains at a given angle for the α-form is almost perpendicular to that for the β-form. Further, the relative intensity difference over the period is more than double for the β-form. This observation is thought to be related to differences in the superstructure of the spherulite. It is well documented that during crystallization of iPP, polymer crystallites grow out radially from the nucleus. In α-iPP, lateral growth or cross-hatching also takes place, with branches growing out tangentially at an angle of around 80° from the radial branch [94–96]. In β-iPP no tangential growth is observed [96], and this may explain the more important intensity differences in the 840 cm^{-1} band as a function of angle, since the average chain orientation is averaged out in the α-form. The spectra recorded at angles of 0° and 90° in a β-spherulite (from the model in Fig. 7a) are shown in Fig. 7c, and are very similar to those reported between 750 and 950 cm^{-1} by Lustiger et al. [97] from directionally

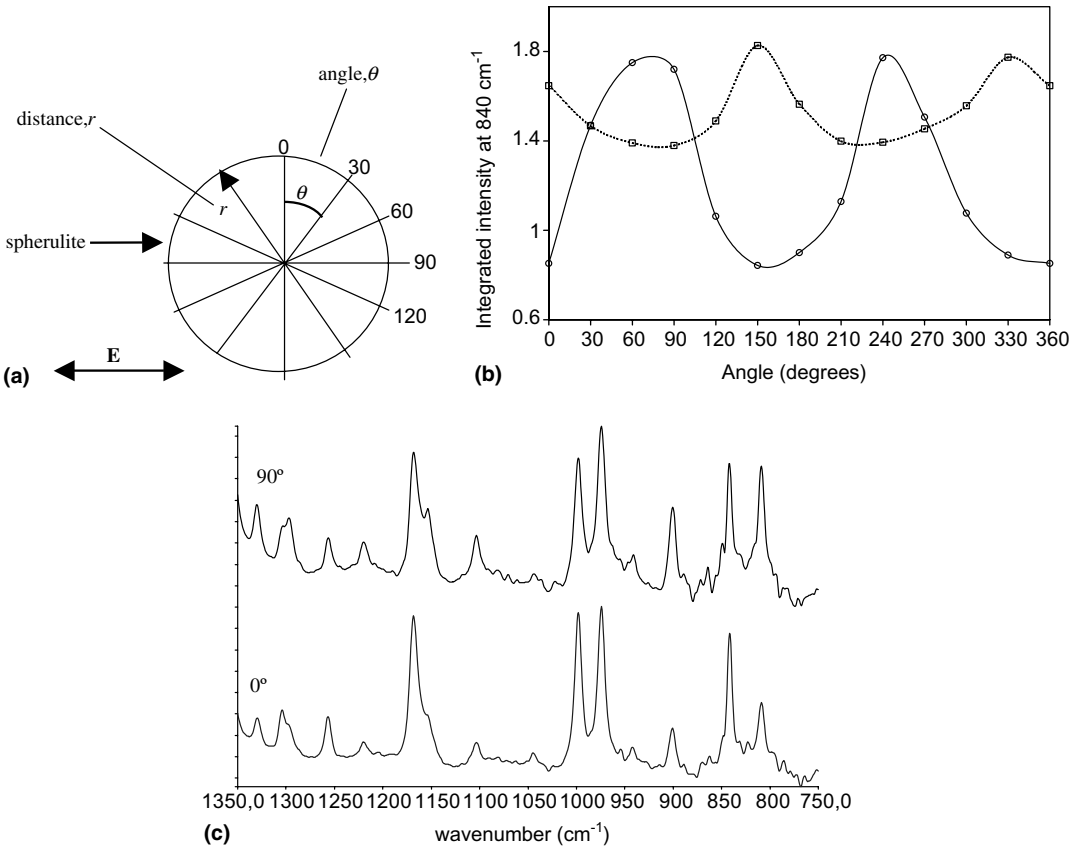

Fig. 7. Synchrotron IR microscopy of α- and β-spherulites; (a) experimental arrangement for single point spectra taken within spherulites, (b) integrated intensity of 840 cm^{-1} band versus measurement angle, and (c) spectra recorded from inside the β-spherulite at angles of 0° and 90°.

crystallized β-iPP films with parallel and perpendicular polarisation.

3.2.2. Transcrystallinity in iPP–LCP fibre composites

Preferentially orientated crystallization of iPP can occur at nucleating surfaces, for example polymer sheets or fibres, where the nucleation density is very high, and the spherulitic growth of adjacently nucleated crystallites leads to almost parallel superstructures within the iPP matrix. This type of epitaxy is termed transcrystallinity, and can be typically observed in fibre-reinforced composites, where it is termed cylindrical growth, Fig. 8. We have studied the nature of transcrystallinity in a series of model composites, and shown by both conventional polarised IR microscopy and by

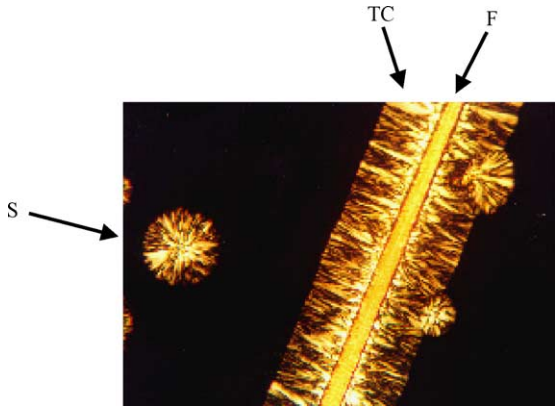

Fig. 8. Polarised optical micrograph of an iPP–LCP fibre composite at 127 °C obtained during dynamic crystallization at 10 °C min. F = LCP fibre, S = developing spherulitic iPP, TC = developing transcrystalline iPP.

synchrotron IR microscopic mapping that it is possible to distinguish between transcrystalline and spherulitic material [79].

The nature of the interphase between reinforcing fibres and the polymer matrix is essential to the mechanical properties of fibre loaded composites, and synchrotron IR microscopy can provide fundamental information in order to understand the microstructure of this region. Under typical processing conditions, the iPP matrix will crystallize predominantly in the α-form. However, during processing shear forces are present, and the transcrystalline layer which forms can be either α or β. The β-form of iPP has higher modulus and a lower crystallinity than the α-form [90,98]. We have studied a series of model composites with both sheared and quiescent fibres in order to differentiate between the α and β transcrystalline structures.

It was pointed out earlier that the variations in a number of bands observed are very sensitive to the morphology. As such, by obtaining a series of spectra with the *E* vector perpendicular and parallel to the fibre axis, we are able to determine from a spectrum the most likely chain polymorphic form and average chain direction for the diffraction limited sampled area. A series of basic rules have been devised from the study of a number of band ratios in preferentially oriented α- and β-iPP [79].

Fig. 9 shows a microphotograph of an area around a sheared fibre, with the electric vector of the synchrotron beam indicated. A series of 125 spectra were recorded with an aperture size of 6 μm, and 3 μm steps along the line indicated. A number of regions can be identified from the spectra and are numbered in the figure. Region 1 corresponds to spherulitic iPP in the α-form, and this can be clearly observed in the photograph. Region 2 corresponds to the β-form of iPP, and region 3 to α-form once again. The spectra in region 4 have a background dominated by the LCP fibre, and region 5 appears to be the α-form. Fig. 10 shows the variation in the relative intensity of the 1296 cm^{-1}/1304 cm^{-1} band pair, with distance across the sample, and corresponds closely to the data in Fig. 9.

In the study of the interphase region of these model composites, one of the most important observations is that in all cases where β transcrystallinity is generated the spectra obtained close

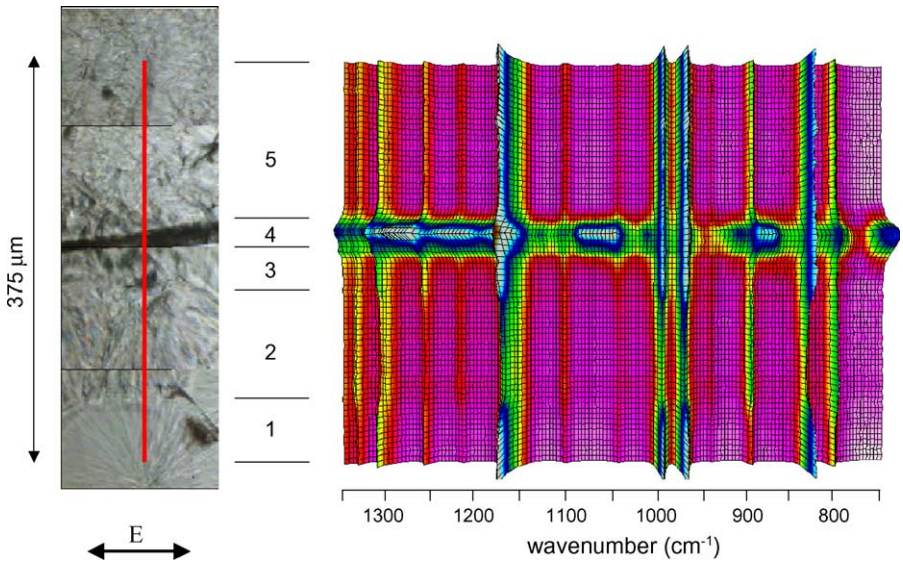

Fig. 9. Mosaic of optical microscope images recorded from an iPP–LCP model composite where the fibre has been sheared at the isothermal crystallization temperature of 140 °C, and pseudo-3D plot of spectra recorded along the line indicated, with an aperture of 6 μm (see text for details).

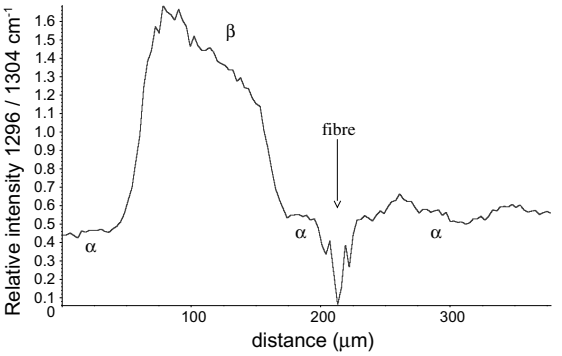

Fig. 10. Variation in the relative intensity for the 1296 cm^{-1}/1304 cm^{-1} band ratio versus distance along the line defined in the model composite in Fig. 9.

to the nucleating fibre appear to correspond to the α-form. This observation can be correlated with a number of morphological studies of fibre reinforced iPP by polarised optical microscopy [90,99], electron and atomic force microscopy [100,101], where it has been accepted that α row nuclei are generated on the fibre surface, and it is these nuclei which give rise to the generation of the β-cylindrical or transcrystalline layer. We recently reported the first structural evidence from synchrotron IR microscopy to corroborate this hypothesis [79], and we have observed this phenomenon with a variety of fibre types and preparation conditions [102].

4. Conclusions

High-resolution diffraction limited transmission infrared microscopy can be performed in an infrared microscope using synchrotron IR radiation. The advantages of the synchrotron IR source have opened up whole new areas in the study of polymer films, and high quality spectra can be obtained with very small apertures, even below the diffraction limit. Examples of several heterogeneous polymer systems based on polypropylene were shown, and synchrotron IR microscopy has been demonstrated to be a very effective tool for the characterization of polymer blends, and different crystalline morphologies observed in an isotactic polypropylene matrix. The complimentary nature of other vibrational microscopy techniques was also shown.

The ability to obtain structural information from inside semicrystalline superstructures is particularly interesting, and can be correlated with morphological measurements from other techniques. Chain orientation and polymorphism has been considered from within polymer spherulites and complex morphologies in fibre reinforced model composites can be elucidated. New structural evidence has been presented for the development of transcrystalline morphologies in sheared and quiescent systems.

Acknowledgements

The authors wish to acknowledge the financial support from the Spanish Government Project, Mat-2002-03831, and the European Community "Enhancing Access to Research Infrastructures", Project IM 008-03 for access to LURE. We wish to thank Prof. Paul Dumas for enthusiastic support in the use of the MIRAGE Beamline, and fruitful discussions. Finally, our thanks to Dr. Robert Alexander and Perkin Elmer Ltd., Seer Green, UK for the use of the Spotlight IR Imaging System, and Dr. Tim Smith and Renishaw plc, Wotton-under-Edge, UK for his help and the use of the confocal Raman microscope.

References

[1] H.L. Dinsmore, Spectrochim. Acta 12 (1959) 1025.
[2] C.E. Weir, E.R. Lippincott, A. Van Valkenburg, E.N. Bunting, J. Res. Natl. Bur. Stand. 63A (1959) 55.
[3] R.M. Badger, R. Newman, Rev. Sci. Instrum. 22 (1951) 935.
[4] E.R. Blount, J. Opt. Soc. Am. 51 (1951) 547.
[5] M.A. Harthcock, L.A. Lentz, B.L. Davis, K. Krishnan, Appl. Spectrosc. 40 (1986) 210.
[6] R.G. Messerschmidt, M.A. Harthcock (Eds.), Infrared Microscopy, Theory and Applications, Practical Spectroscopy Series, vol. 6, Marcel Dekker, New York, 1988.
[7] F.J. Bergin, Appl. Spectrosc. 43 (1989) 511.
[8] K. Krishnan, S.L. Hill, FT-IR Microsampling Techniques, Practical Fourier Transform Infrared Spectroscopy, Academic Press, New York, 1990 (Chapter 3).
[9] J.E. Katon, Vibr. Spectrosc. 7 (1994) 201.
[10] J.M. Chalmers, N.J. Everall, Macromol. Symp. 94 (1995) 33.

[11] H.J. Humecki (Ed.), Practical Guide to Infrared Microspectroscopy, Practical Spectroscopy Series, vol. 19, Marcel Dekker, New York, 1996.
[12] E. Abbe, Mikrosk. Anat. 9 (1873) 413.
[13] J.A. Bailey, R.B. Dyer, D.K. Graff, J.R. Schoonover, Appl. Spectrosc. 54 (2000) 159.
[14] G. Turrell, J. Corset, Raman Microscopy: Developments and Applications, Academic Press, 1996.
[15] R.F. Egerton, Electron Energy-Loss Spectroscopy in the Electron Microscope, second ed., Plenum Press, 1996.
[16] J. Stöhr, NEXAFS Spectroscopy Springer Series in Surface Sciences, No. 25, Springer Verlag, 1996.
[17] B.D. Ratner, V.V. Tsukruk (Eds.), Scanning Probe Microscopy of Polymers, ACS Symposium Series, 694, American Chemical Society, 1998.
[18] K. Varlot, J.M. Martin, C. Quet, Y. Kihn, Ultramicroscopy 68 (1997) 123.
[19] K. Varlot, J.M. Martin, D. Gonbeu, C. Quet, Polymer 40 (1999) 5691.
[20] S. Horiuchi, T. Hamanaka, T. Aoki, T. Miyakawa, R. Narita, H. Wakabayashi, J. Electron. Microsc. 52 (2003) 255.
[21] C. Park, R.E. Crooks, E.J. Siochi, J.C. Harrison, N. Evans, E. Kenik, Nanotechnology 14 (2004) L11.
[22] H. Ade, X. Zhang, S. Cameron, C. Costello, J. Kirz, S. Williams, Science 258 (1992) 972.
[23] H. Ade, S.G. Urquhart, NEXAFS spectroscopy and microscopy of natural and synthetic polymers, in: T.K. Sham (Ed.), Chemical Applications of Synchrotron Radiation, World Scientific Publishing, Singapore, 2002.
[24] A.P. Hitchcock, J. Synchr. Radiat. 8 (2001) 66.
[25] H. Ade, B. Hsaio, Science 262 (1993) 1427.
[26] A.P. Smith, H. Ade, Appl. Phys. Lett. 69 (1996) 3833.
[27] A. Cossy-Favre, J. Diaz, Y. Liu, H. Brown, M.G. Samant, J. Stöhr, A.J. Hanna, S. Anders, T.P. Russel, Macromolecules 31 (1998) 4957.
[28] A.L.D. Kilcoyne, T. Tylisczak, M. Kritcher, Peter Hitchcock, S. Fakra, K. Frank, C. Zimba, M. Rafailovich, J. Sokolov, G. Cody, E. Rightor, G. Mitchell, I. Koprinarov, E. Anderson, B. Harteneck, A. Hitchcock, T. Warwick, H. Ade, ALS News, Fall 2001. Available from: <http://www.physics.ncsu.edu/stxm/p-stxm-first-results.pdf> (Accessed: 01/07/2004).
[29] A. Cricenti, Appl. Surf. Sci. 162 (2000) 275.
[30] D.A. Smith, S. Webster, M. Ayad, S.D. Evans, D. Fogherty, D.N. Batchelder, Ultramicroscopy 61 (1995) 247.
[31] M.S. Anderson, W.T. Pike, Rev. Sci. Instrum. 73 (2002) 1198.
[32] B. Knoll, F. Kielmann, Nature 399 (1999) 134.
[33] F. Kielmann, Vibr. Spectrosc. 29 (2002) 109.
[34] A. Lahrech, R. Bachelot, P. Gleyzes, A.C. Boccara, Opt. Lett. 21 (1996) 1315.
[35] C.A. Michaels, S.J. Stranick, L.J. Richter, R.R. Cavenagh, J. Appl. Phys. 88 (2000) 4832.
[36] A. Hammiche, H.M. Pollock, M. Reading, M. Claybourn, P.H. Turner, K. Jewkes, Appl. Spectrosc. 53 (1999) 810.
[37] L. Bozec, A. Hammiche, H.M. Pollock, M. Conroy, J.M. Chalmers, N.J. Everall, L. Turin, J. Appl. Phys. 90 (2001) 5159.
[38] G.P. Williams, Nucl. Instr. and Meth. 195 (1982) 383.
[39] W.D. Duncan, G.P. Williams, Appl. Opt. 22 (1983) 2914.
[40] G.L. Carr, P. Dumas, C.J. Hirschmugl, G.P. Williams, Il Nuovo Cimento 20 (1998) 375.
[41] J.A. Reffner, P.A. Martoglio, G.P. Williams, Rev. Sci. Instrum. 66 (1995) 1298.
[42] G.L. Carr, J.A. Reffner, G.P. Williams, Rev. Sci. Instrum. 66 (1995) 1490.
[43] G.L. Carr, M. Hanfland, G.P. Williams, Rev. Sci. Instrum. 66 (1995) 1643.
[44] M. Jackson, H.H. Mantsch, J. Mol. Struct. 408–409 (1997) 105.
[45] N. Jamin, P. Dumas, J. Moncuit, W.H. Fridman, J.L. Teillaud, G.L. Carr, G.P. Williams, Proc. Natl. Acad. Sci. USA 95 (1998) 4837.
[46] D.L. Wetzel, S.M. LeVine, Science 285 (1999) 1224.
[47] J.L. Bantignies, G.L. Carr, D. Lutz, S. Marull, G.P. Williams, G. Fuchs, J. Cosmetic Sci. 51 (2000) 73.
[48] H.L. Holman, M.C. Martin, E.A. Blakely, K. Bjornstad, W.R. McKinney, Biopolymers 57 (2000) 329.
[49] L. Kreplak, F. Briki, Y. Duvault, J. Doucet, C. Merigoux, F. Leroy, J.L. Lévêque, L. Miller, G.L. Carr, G.P. Williams, P. Dumas, Int. J. Cosmetic Sci. 23 (2001) 369.
[50] L.M. Miller, T.J. Tague, Vibr. Spectrosc. 28 (2002) 159.
[51] P. Dumas, L. Miller, J. Biol. Phys. 29 (2003) 201.
[52] L.M. Miller, G.D. Smith, G.L. Carr, J. Biol. Phys. 29 (2003) 219.
[53] L.M. Miller, P. Dumas, N. Jamin, J.L. Teillaud, J. Miklossy, L. Forro, Rev. Sci. Instrum. 73 (2002) 1357.
[54] K. Theodore, M.C. Martin, Planta 213 (2001) 881.
[55] P. Bouchon, P. Hollins, M. Pearson, D.L. Pyle, M.J. Tobin, J. Food Sci. 66 (2001) 918.
[56] O. Piot, J.-C. Autran, M. Manfait, J. Cereal Sci. 34 (2001) 191.
[57] D.L. Wetzel, P. Srivarin, J.R. Finney, Vibr. Spectrosc. 31 (2003) 109.
[58] N. Guilhaumou, P. Dumas, G.L. Carr, G.P. Williams, Appl. Spectrosc. 52 (1998) 1029.
[59] H.Y.N. Holman, D.L. Perry, M.C. Martin, G.M. Lamble, W.R. McKinney, J.C. Hunter-Cevera, Geomicrobiol. J. 16 (1999) 307.
[60] P.I. Raynal, E. Quirico, J. Borg, D. Deboffle, P. Dumas, L. d'Hendecourt, J.-P. Bibring, Y. Langevin, Planet. Space Sci. 48 (2000) 1329.
[61] J.T. Geller, H.-Y. Holman, G. Sua, M.E. Conrad, K. Pruess, J.C. Hunter-Cevera, J. Contam. Hydrol. 43 (2000) 63.
[62] M. Glerup, G.O. Sorensen, P. Beichert, M.S. Johnson, Spectrochim. Acta A 58 (2002) 129.
[63] G.P Halada, C.R. Clayton, State-of-the-art application of surface and interface analysis methods to environmental material interactions, Proc. Electrochem. Soc. 2001-5 (2001) 149–162.

[64] X. Zhang, P.N. Ross, R. Kostecki, F. Kong, S. Sloop, J.B. Kerr, K. Striebel, E.J. Cairns, F. McLarnon, J. Electrochem. Soc. 148 (2001) A463.
[65] P. Dumas, G.P. Williams, Chemical applications of synchrotron radiation, Part 1, Adv. Ser. Phys. Chem. 12A (2002) 356.
[66] R.J. Hemley, A.F. Goncharov, R. Lu, V.V. Struzhkin, M. Li, H.K. Mao, Il Nuovo Cim. Soc. Ital. Fis. D 20 (1998) 539.
[67] Z. Liu, J. Hu, H. Yang, H.K. Mao, R.J. Hemley, J. Phys.: Condens. Matter 14 (2002) 10641.
[68] J.L. Bantignies, G. Fuchs, G.L. Carr, P. Dumas, C. Wilhelm, Accelerator-based infrared sources and applications, Proc. SPIE-Int. Soc. Opt. Eng. 3153 (1997) 125.
[69] G.L. Carr, P. Dumas, L.M. Miller, G.P. Williams, Synchr. Radiat. News 11 (1998) 31.
[70] J.L. Bantignies, G. Fuchs, G.L. Carr, G.P. Williams, D. Lutz, S. Marull, Int. J. Cosmet. Sci. 20 (1998) 381.
[71] T.J. Wilkinson, D.L. Perry, M.C. Martin, W.R. McKinney, A.G. Thompson, Abstr. Pap. Am. Chem. Soc. 222 (2001) 36-IEC.
[72] T.J. Wilkinson, D.L. Perry, M.C. Martin, W.R. McKinney, A.G. Thompson, Abstr. Pap. Am. Chem. Soc. 223 (2001) 78-IEC.
[73] T.J. Wilkinson, D.L. Perry, M.C. Martin, W.R. McKinney, A.A. Cantu, Appl. Spectrosc. 56 (2002) 800.
[74] G.L. Carr, Vibrat. Spectrosc. 19 (1999) 53.
[75] P. Dumas, G.L. Carr, G.P. Williams, Analusis, Eur. J. Anal. Chem. 28 (2000) 68.
[76] J.A. Reffner, G.L. Carr, G.P. Williams, Mikrochim. Acta (Suppl.) 14 (1997) 339.
[77] J.M. Chalmers, N.J. Everall, K. Hewitson, M.A. Chesters, M. Pearson, A. Grady, B. Ruzicka, Analyst 123 (1998) 579.
[78] G. Ellis, C. Marco, M.A. Gómez, E.P. Collar, J.M. García-Martínez, J. Macromol. Sci. Phys. B43 (2004) 253.
[79] G. Ellis, C. Marco, M.A. Gómez, J. Macromol. Sci. Phys. B43 (2004) 191.
[80] C. Marco, M.A. Gómez, G. Ellis, J.M. Arribas, J. Appl. Polym. Sci. 84 (2002) 1669.
[81] C. Marco, G. Ellis, M.A. Gómez, J.G. Fatou, J.M. Arribas, I. Campoy, A. Fontecha, J. Appl. Polym. Sci. 65 (1997) 2665.
[82] R. Hoult, R. Spragg, Int. J. Vibr. Spectrosc. 6 (2) (2002) 4, Available from: <www.ijvs.com>.
[83] F. Polack, R. Mercier, L. Nahon, C. Armellin, J.P. Marx, M. Tanguy, M.E. Couprie, P. Dumas, Accelerator-based sources of infrared and spectroscopic applications, Proc. SPIE 3775 (1999) 13.
[84] C. Marco, G. Ellis, M.A. Gómez, J.M. Arribas, Activity of different nucleating agents on the crystallisation behaviour of isotactic polypropylene and its impact on some mechanical properties, in: S.G. Pandalai (Ed.), Recent Research Developments in Applied Polymer Science, vol. 1, Part II, Transworld Research Network, Kerala, 2002, pp. 587–610.
[85] C.M. Snively, J.L. Koenig, J. Polym. Sci. Part B: Polym. Phys. 37 (1999) 2353.
[86] G. Ellis, Macromol. Symp. 184 (2002) 37.
[87] G.L. Carr, Rev. Sci. Instrum. 72 (2001) 1613.
[88] D.I. Bower, W.F. Maddams, The Vibrational Spectroscopy of Polymers, Cambridge University Press, Cambridge, 1989, p. 165 (Chapter 5).
[89] L.G. Tisinger, A.J. Sommer, Appl. Spectrosc. 56 (2002) 1397.
[90] J. Varga, Crystallization, melting and supermolecular structure of isotactic polypropylene, in: J. Karger-Kocsis (Ed.), Polypropylene. Structure, Blends and Composites, vol. 1, Structure and Morphology, Chapman & Hall, London, 1995, pp. 56–115.
[91] G. Ellis, M.A. Gómez, C. Marco, Int. J. Vibr. Spectrosc. 5 (4) (2001) 7.
[92] T. Miyazawa, J. Polym. Sci. Part C 7 (1964) 59.
[93] P.G. Schmidt, J. Polym. Sci. A 1 (1963) 2317.
[94] D.R. Norton, A. Keller, Polymer 26 (1985) 704.
[95] B. Lotz, J.C. Whitman, A.J. Lovinger, Polymer 37 (1996) 4979.
[96] E. Nedkov, T. Dobreva, e-Polymers 42 (2002) 1.
[97] A. Lustiger, C.N. Marzinsky, R.R. Mueller, H.D. Wagner, J. Adhes. 53 (1995) 1.
[98] Ph. Tordjeman, C. Robert, G. Marin, P. Gerard, Eur. Phys. J. E 4 (2001) 459.
[99] J. Varga, J. Karger-Kocsis, J. Polym. Sci. Part B: Polym. Phys. 34 (1996) 657.
[100] C.M. Wu, M. Chen, J. Karger-Kocsis, Polym. Bull. 41 (1998) 493.
[101] C.M. Wu, M. Chen, J. Karger-Kocsis, Polymer 40 (1999) 4195.
[102] G. Ellis, unpublished results.